



much longer than for 2D single-shot sequences, free-breathing with navigator technique has to be applied. When steady breathing can be accomplished by the patient, a high-resolution dataset is obtained in 3–6 minutes and, if parallel imaging is employed, even faster. A technical highlight of 3D sequences for MRCP is the use of a restore pulse. When the last echo during a turbo-spin acquisition has been recorded, another 180° pulse is used to refocus the remaining transverse magnetization, but instead of acquiring the echo, a subsequent 90° pulse is used to flip the transverse magnetization back to the z-axis. Thus the magnetization is restored much faster than relying on the natural T1-relaxation. After an interval of several repetition times, a steady state of longitudinal magnetization is established with net enhancement of the long T2-components. In this manner, signals from fluid can be enhanced dramatically in these images [6]. Although the rather long acquisition of 3D-TSE sequences renders them susceptible for motion artifacts, according to our experiences, im-

ages of excellent quality can be obtained in the vast majority of patients. It is the combination of high spatial resolution and a high contrast-to-noise ratio for fluids that make these images the ideal starting point for advanced post-processing and visualization.

### Post-processing

It is the ongoing evolution of hardware and software that brings highly sophisticated post-processing techniques from the ivory tower of high performance computer labs to our everyday working place. The combination of reconstructed image stacks and interactive visualization gives us the possibility of exploring complex datasets and define and optimize the presentation of regions-of-interest and different image characteristics after the examination has been completed. The standard post-processing tools that are available on a variety of workstation and server-client solutions mainly comprise multiplanar-reformation (MPR), maximum intensity projection (MIP), and volume rendering techniques (VRT). Al-

though originally applied to CT data, the ability of MRI to create images with high resolution and uniformly high contrast for vessels or other distinct anatomical structures now allows for a combination of both techniques.

### Image Gallery

In our opinion, MRCP – especially the use of volume rendering and perspective volume rendering – opens up a new way of looking at MRI data that not only fascinates the clinician but also allows a comprehensive visualization of the examination for the radiologist, sometimes indicating changes that could have been missed on source images. It has to be kept in mind, however, that this kind of post-processing will always lead to a reduction of information compared to the source data. Therefore a thorough review of these images cannot be omitted. All presented images were acquired with a 1.5T scanner (MAGNETOM Avanto, Siemens, Erlangen, Germany) and post-processed on a dedicated workstation.

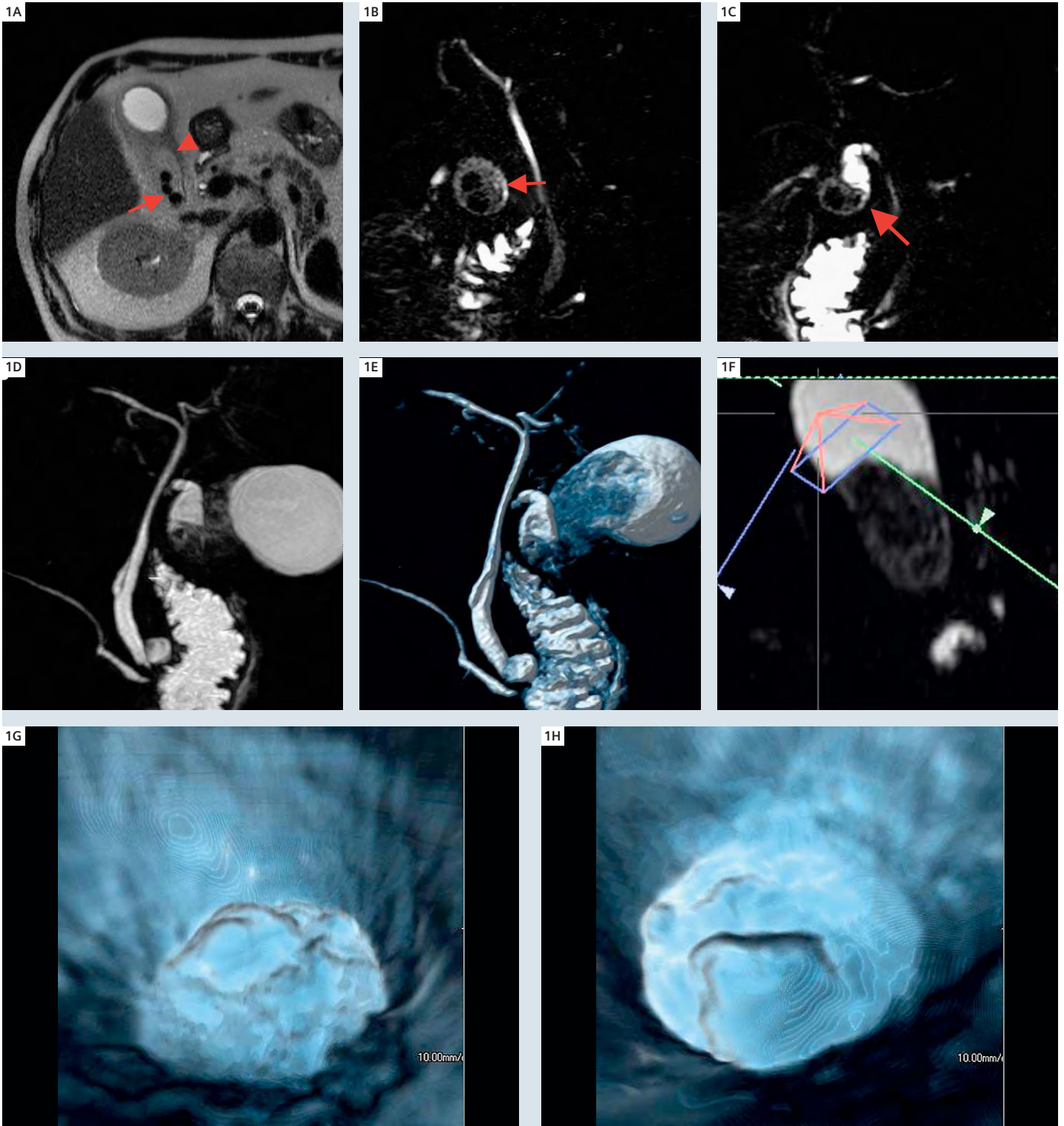
### Case 1: Gallstones

A 58-year-old male patient was referred for MRI of the liver and biliary tract after experiencing an episode of severe upper abdominal pain. Liver enzymes were slightly elevated. Ultrasonography was initially performed and showed cholecystolithiasis, but clear visualization of the wall of the gallbladder and the neighboring tissue could not be achieved due to superimposing structures. Although acute cholecystitis was already suspected, MRCP was performed to exclude other causes of enzyme elevation.

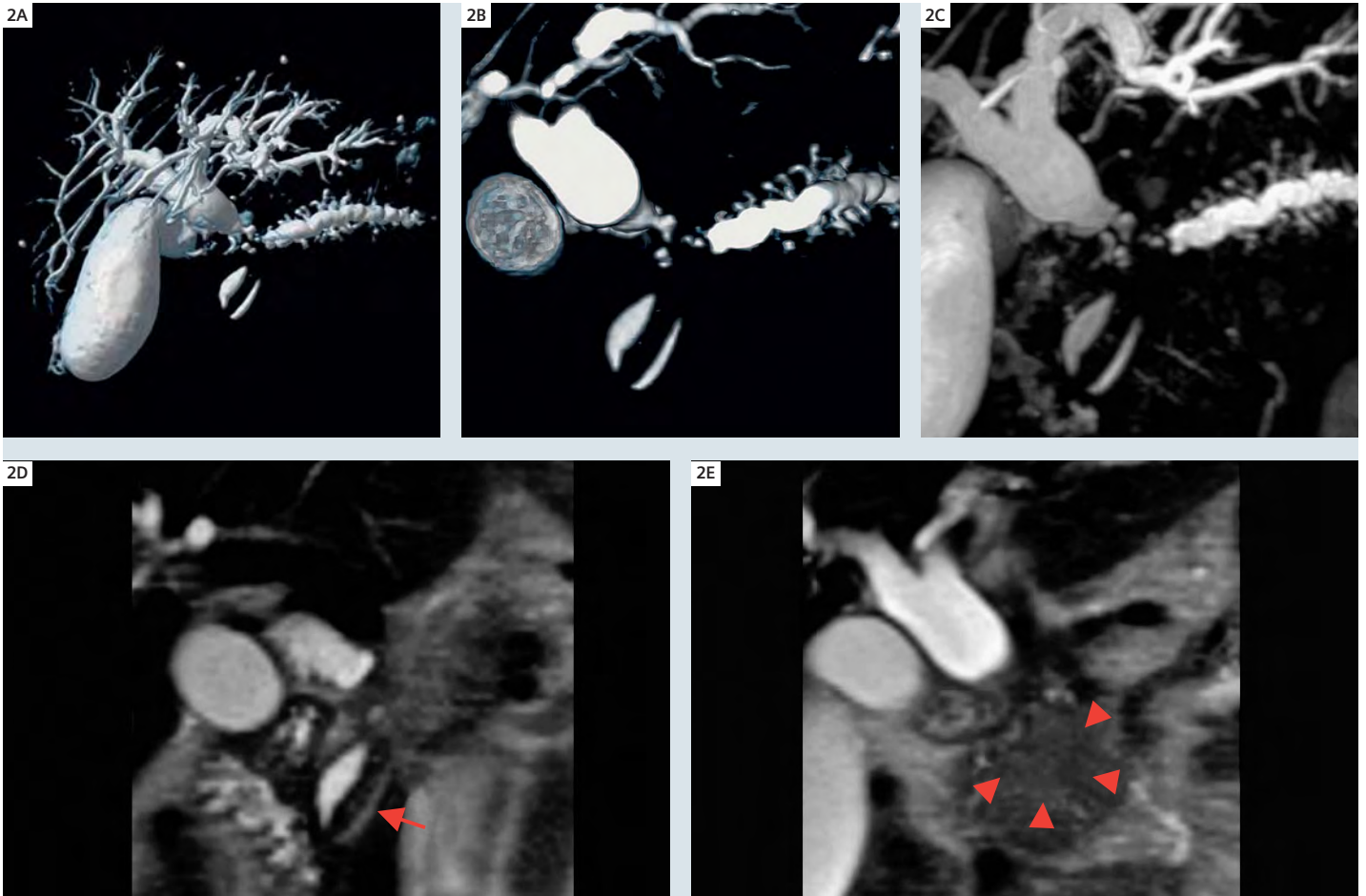
(A) An axial HASTE image shows sludge (arrowhead) three stones (arrow) in the

gallbladder. A thickened wall can be noted as a sign of the acute inflammation. (B) A coronal source image from the 3D TSE sequence shows a section through the gallbladder with sludge (inhomogeneous low signal) and two stones (arrow). The intrahepatic and extrahepatic bile ducts appear normal. (C) A paracoronar MPR of the 3D TSE shows stones and sludge in the neck of the gallbladder, but the cystic duct remains free of concretions. (D and E) MIP (D) and VRT (E) of the 3D TSE sequence nicely depict the biliary and pancreatic ducts. The sludge and stones

can be recognized as filling defects of the gallbladder, but differentiation between stones and sludge is impossible due to the low signal of both entities. Image orientation represents a posterior view. (F) Shows a planning image for perspective VRT. A set of three perpendicular MPR images (only one shown here) is used to place a camera-like point on which the ray-tracing paths are centered to create a virtual endoscopy view. (G and H) Two virtual views using perspective VRT from the top of the gallbladder onto the sludge and the stones rising above this level, as icebergs in the sea.



1 Case 1: Gallstones



2 Case 2: Pancreatic cancer

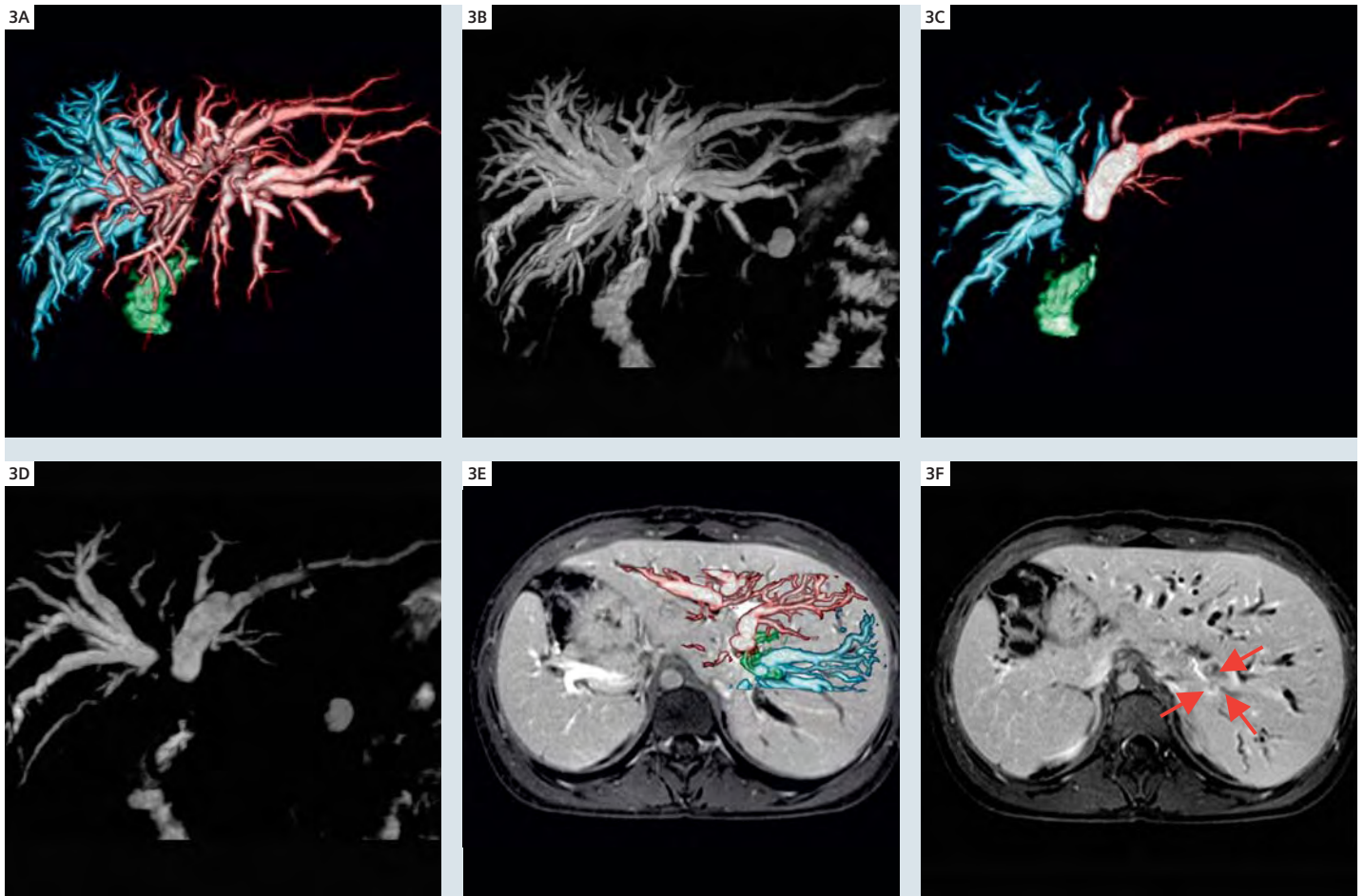
## Case 2: Pancreatic cancer

A 65-year-old female patient was referred to our oncology department due to weight-loss and recently developed jaundice. Ca19-9 as a tumor marker for e.g. pancreatic carcinoma was elevated over 3000 U/ml. She received an MRI scan of the pancreas and biliary tract in search of a pancreatic neoplasm.

(A) A VRT of the 3D TSE sequence shows markedly dilated intrahepatic and pancreatic ducts. Distal to the cystic duct in the upper part of the pancreatic head both

biliary and pancreatic ducts almost completely terminate. Shortly below this area both ducts can again be delineated with normal caliber down to the papilla. (B) An enlarged view of the defect of both ducts with a coronal cut-plane through the proximal part of the common bile duct and the pancreatic duct shows the conic stump of the bile duct and the tremendous dilation of both systems with even the small side-branches of the pancreatic duct being clearly visible down

to third order branches. (C) A MIP image in the same orientation as (B) depicts the findings with even higher clarity and resolution but with a weaker 3-dimensional impression. (D and E) Coronal HASTE images parallel to the cut-plane in (B). In (D) the distal parts of both ducts can be seen (arrow). In (E), two slices dorsal to (D), a neoplasm in the pancreatic head can be noted (arrowheads) that abuts the duodenum and the biliary tract.



**3** Case 3: Klatskin tumor

### Case 3: Klatskin tumor

A 22-year-old female patient with jaundice and no upper abdominal pain. MRI of the upper abdomen was conducted as part of a thorough work-up.

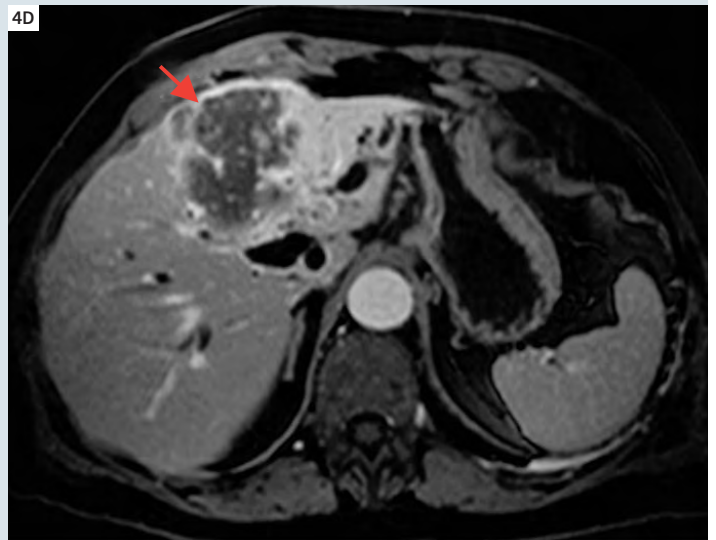
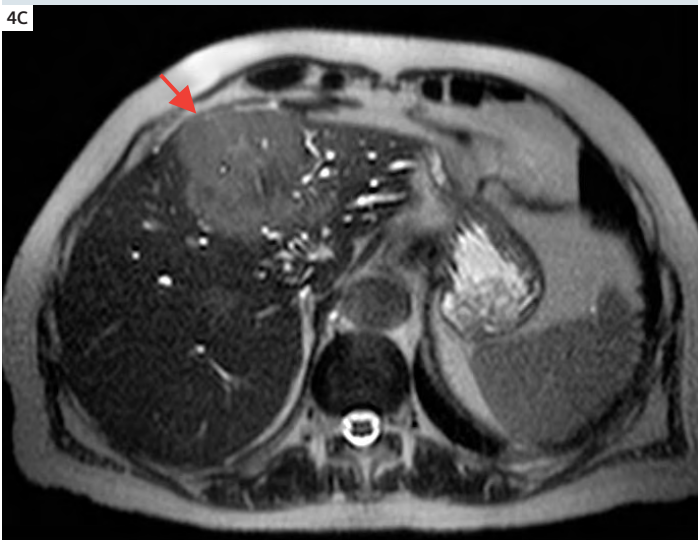
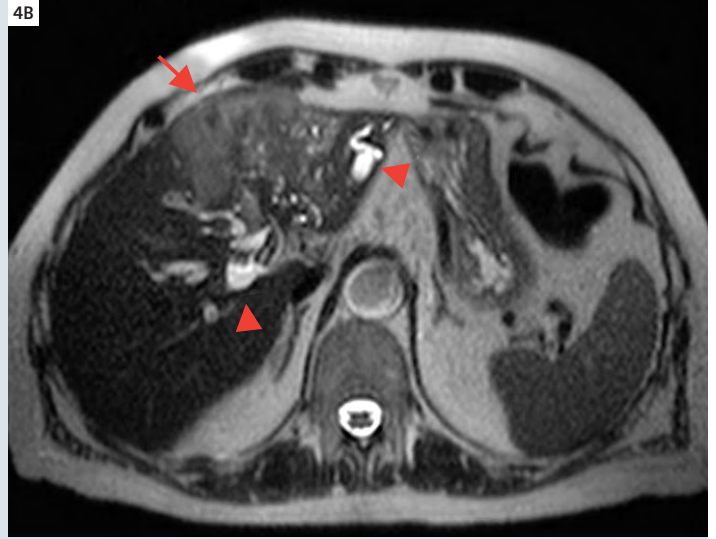
(A and B) VRT (A) and MIP (B) images reconstructed from the 3D TSE sequence. For the VRT manual segmentation were used in the source slices to identify right and left hepatic duct system as well as the remaining parts of the extrahepatic system. Segmentation information was combined with different color-coded transfer functions (right = blue; left = red; extrahepatic = green), allowing better identification of the anatomy when slabs and cut-planes are used (see C to F). All intrahepatic bile ducts show marked dilation.

(C and D) Same images as (A) and (B), but with a paracoronal cut-plane (A) or a paracoronal slab selection (B; 1.5 cm) to gain better view of the central parts of the biliary tree. Note the conic abrogation of both hepatic ducts proximal to the common bile duct. Remnants of the common bile duct and the gallbladder are present more distally.

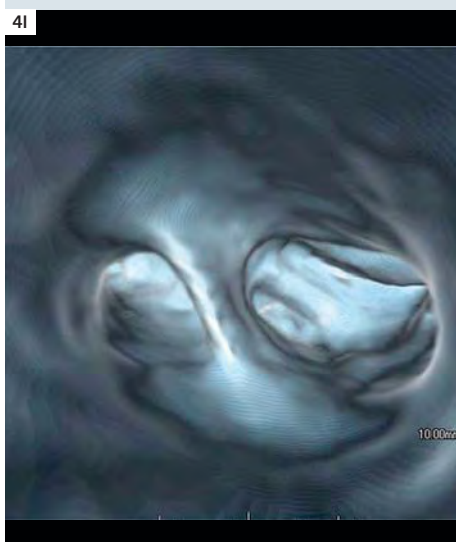
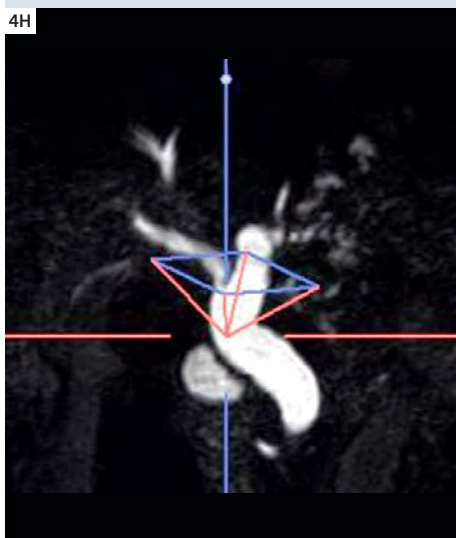
(E) Here we manually superimposed an axial slab from the color-coded VRT with an axial contrast-enhanced gradient-echo sequence. The image orientation of the axial sequence was mirrored to maintain a "view from above", as is normally used with VRT instead of the classic radiological view of slice data. The correlation with

anatomic information further strengthens the localization of the stenoses in the region where left and right hepatic system normally join to form the common bile duct.

(F) An image from the same series of contrast-enhanced images as in (E) just two slices lower. In the region of the ductal stenoses a hypointense lesion with rim-enhancement can be delineated (arrowheads). After histological sampling the diagnosis of a Klatskin tumor could be confirmed. Unfortunately resection was considered impossible as the MRI showed gross involvement of the left and right biliary systems.



4 Case 4: Intrahepatic cholangiocarcinoma



## Case 4: Intrahepatic cholangiocarcinoma

An 80-year-old male patient was referred to our department after repeated episodes of hepatolithiasis and a suspected mass in the left liver lobe.

(A–C) Three consecutive slices from an axial HASTE sequence show a large hyperintense and ill-defined mass (arrow) arising from the left liver lobe causing dilation of the adjacent ductal structures (arrowheads). Whereas slice A and B can clearly be delineated as consecutive images, slice C represents a markedly different anatomic position. Due to this offset in position the bile ducts and other anatomic structures cannot easily be traced in through-plane direction. This offset in image position is known as “serious misregistration artifact” and represents a major drawback of breath-hold HASTE imaging. (D) Shows a image from an axial contrast-enhanced gradient-echo sequence. The large tumor can be identified as a hypointense multilobulated structure with rim-enhancement. Histological work-up confirmed the diagnosis of an intrahepatic cholangiocarcinoma.

(E–G) RARE (E) and 3D-TSE images as VRT (F) and MIP (G) all nicely show the disruption of the intrahepatic bile ducts in the left lobe concomitant with dilation of the residual ducts. The presence of a pancreas divisum with the common bile duct and the pancreatic duct opening to different papillae can, although visible in all images, best be identified in the VRT (arrowheads). The MIP also shows the actual finding, but does not provide further depth-information. The MRCP image is impaired by fluid overlay from the stomach and duodenal bulb.

(H and I) A manually angulated MPR of the 3D-TSE images in a paracoronal orientation (H) shows a section through the common bile duct in a comparable position to images E–G. This image is used to plan the “camera position” for the virtual VRT (I) that shows an endoluminal view on the main branching of the bile duct.

## References

- 1 Rosch T, Meining A, Fruhmorgen S et al. A prospective comparison of the diagnostic accuracy of ERCP, MRCP, CT, and EUS in biliary strictures. *Gastrointest Endosc* 2002 ; 55: 870–876.
- 2 Wallner BK, Schumacher KA, Weidenmaier W, et al. Dilated biliary tract: evaluation with MR-cholangiography with a T2-weighted contrast enhanced fast sequence. *Radiology* 1991; 181: 805–808.
- 3 Hennig J, Nauerth A, Friedburg H. A fast imaging method for clinical MR. *Magn Reson Med* 1986; 3:823-833.
- 4 Wallnoefer AM, Herrmann KA, Beuers U, et al. Comparison of 2D and 3D sequences for MRCP. Clinical value of the different techniques. *Radiologe* 2005; 45(11): 996-1003.
- 5 Bley TA, Pache G, Saueressig U, et al. State of the Art 3D MR-Cholangiopancreatography for Tumor Detection. *In vivo* 2007; 21(3).
- 6 Augui J, Vignaux O, Argaud C, et al. Liver: T2-weighted Imaging with Breath-hold Fast-Recovery Optimized Fast Spin-Echo Compared with Breath-hold Hald-Fourier and Non-Breath-hold Respiratory-triggered Fast Spin-Echo Pulse Sequences. *Radiology* 2002; 223(3):853-9.

4 Case 4: Intrahepatic cholangiocarcinoma